CHINESE OPTICS LETTERS

Vol. 23, No. 1 | January 2025

Nano-thick SiO_2 channel for subwavelength plasmonic orbital angular momentum mode transmission

Zhishen Zhang (张智深)[1,†], Xiaobo Heng (衡小波)[2,†], Shuai Gao (高 帅)[1], Li Zhang (张 莉)[1], Fei Lin (林 飞)[1], Weicheng Chen (陈伟成)[1*], and Jiulin Gan (甘久林)[3**]

[1] Guangdong-Hong Kong-Macao Joint Laboratory for Intelligent Micro-Nano Optoelectronic Technology, School of Physics and Optoelectronic Engineering, Foshan University, Foshan 528225, China

[2] GBA Branch of Aerospace Information Research Institute, Chinese Academy of Sciences, Guangzhou 510700, China

[3] State Key Laboratory of Luminescent Materials and Devices and Institute of Optical Communication Materials, South China University of Technology, Guangzhou 510640, China

[†]These authors contributed equally to this work.

*Corresponding author: chenwch@fosu.edu.cn

**Corresponding author: msgan@scut.edu.cn

Received May 24, 2024 | Accepted July 16, 2024 | Posted Online December 27, 2024

Orbital angular momentum (OAM) waveguides are critical for multi-channel photonic-on-chip applications. However, current large-mode-area waveguides pose a challenge for OAM device miniaturization. Here, a novel hybrid plasmonic waveguide is theoretically proposed to decrease the OAM mode area by two orders of magnitude. Benefiting from the Ag-As_2S_3-SiO_2-As_2S_3-Ag five-layer cylindrical structure, the guided OAM mode realizes a larger figure of merit of 88. Based on this waveguide, an OAM coupler with a record-breaking small footprint (0.68 μm × 5.7 μm) is designed. The proposed waveguide enables subwavelength OAM light transmission, which provides a key building block for high-density OAM photonics circuits.

Keywords: orbital angular momentum waveguide; hybrid plasmonic waveguide; directional coupler.
DOI: 10.3788/COL202523.013601

1. Introduction

The nano-waveguide with non-diffraction-limited light transport has become increasingly critical for applications in many fields, such as chip-scale optical communication[1], trace biochemical sensors[2], and scalable quantum computation[3]. However, a dielectric waveguide with a subwavelength diameter cannot achieve the mode confinement below the diffraction limit since the fraction of evanescent fields dramatically increases with the decreasing waveguide diameter[4]. For constraining the light field into a smaller volume, both metallic waveguides[5,6] and hybrid waveguides[6,7] have been proposed. At the metal–insulator interfaces, the light is strongly coupled with the free electrons of the metal and excites the surface plasmon wave, which highly confines the light in nanoscale. Compared with all-metallic waveguides, the dielectric-metal hybrid waveguide[6,7] tailors the penetration of surface plasmon modes in the dielectric layer and the metal layer, which reduces the ohmic loss and still confines light at smaller scales. Various kinds of nano-waveguides, such as metallic nanowires[8] and grooves[9], hybrid plasmonic waveguides[10,11], and graphene-loaded structures [12], have been theoretically designed and experimentally demonstrated with the ability to confine light below the diffraction limit. However, the above waveguides are only applicable for dealing with the fundamental mode.

In comparison to the fundamental mode, orbital angular momentum (OAM) modes[13] with a helical wavefront and doughnut spot have experienced significant growth in recent years due to their spatial orthogonality, which offers an additional degree of freedom for optical multiplexing[14–17], multi-parameter sensing[18], and spin–orbit interaction[19]. However, OAM waveguides below the diffraction limit are still challenging, which seriously hamper the development of on-chip OAM modulations and communications[20,21]. Currently, only a few strongly confining OAM waveguides have been proposed. In dielectric approaches, cylindrical microfibers[22], rectangular waveguides[23,24], and subwavelength-hole waveguides[25] were designed for guiding OAM modes with negligible loss, and all achieved a mode area at the level of λ^2. As the alternative metallic approaches, a plasmonic nanohole waveguide[26] was proposed for propagating OAM modes with a loss of 2.73 dB/μm and mode area of $0.44\lambda^2$. The plasmonic helical nanowire[27,28] was designed to confine OAM modes into the area of $0.03\lambda^2$. Further confining the OAM mode into nanoscale is much more challenging. For example, the OAM mode in a tapered metal waveguide[29] can be focused into a nanotip but is rapidly

scattered to the far-field. The main challenges arise from three aspects. First, because OAM modes are high-order modes, the size of the OAM waveguide is inherently larger than the size of the corresponding single-mode waveguide. Second, the annular OAM beam has higher stability in a circularly symmetric waveguide, which means the extremely sharp microstructural features in the most single-mode nano-waveguides cannot be used for reference. Third, a nanoscale OAM mode should be located in the dielectric region for achieving low loss, so a hybrid plasmonic waveguide needs to be designed with the optimal combination pattern of both dielectric layers and metal layers. Up to now, there is still no reported OAM waveguide synchronously achieving a nanoscale mode area and a micro-scale propagation range.

In this work, we propose a novel OAM nano-waveguide with a mode area of $0.0005\lambda^2$, which corresponds to decreasing the mode area by 2 orders of magnitude. Enlightened by the mode manipulation techniques in multi-cladding fibers, the light will be highly confined into a tiny dielectric region, which is surrounded by a high-index dielectric layer and a metal layer. The designed OAM waveguide has an ultrathin SiO_2 cylindrical layer acting as the OAM guiding channel, which is clamped at the middle of two As_2S_3 layers and two Ag layers. The OAM mode is more strongly confined in the SiO_2 layer with a relatively long propagation length (2λ to 11λ) and a larger figure of merit (FoM = 88). Based on the subwavelength OAM waveguide, a plasmonic OAM waveguide coupler is demonstrated with a record-breaking small footprint 0.68 μm × 5.7 μm. Due to the efficient constraint mechanism of light fields, two tightly arranged waveguides had a low crosstalk of −28.14 dB. Our plasmonic OAM nano-waveguide holds great potential as a component for the on-chip OAM communications.

2. Theoretic Analysis

The three-dimensional (3D) and cross-sectional schematic configurations of our proposed OAM nano-waveguide are shown in Figs. 1(a) and 1(b). The OAM nano-waveguide consists of a low-index dielectric ring-core, two high index dielectric claddings, and two metal claddings. The radius of the ith layer (from inside to outside) is r_i. It is worth noting that the evanescent field of the subwavelength dielectric waveguide is mostly located in the low-index cladding, instead of the high-index core. For example, the 216 nm diameter silicon wire[30] at 1.5 μm wavelength only confines 10% energy inside the core and 90% energy in the air. Therefore, building the composite structure of the dielectric layer offers a new approach to control the mode distribution of a hybrid waveguide. For example, the light will be confined at the metal–dielectric interface due to the localization effect of the surface plasmon wave. By setting a low-index dielectric nano-structure near the metal–dielectric interface, most energy of the light will be compressed into this nano-structure. In our designed nano-waveguide, the guided modes are tightly restricted in the ultrathin low-index dielectric ring-core channel, which is sandwiched between two high-index dielectric

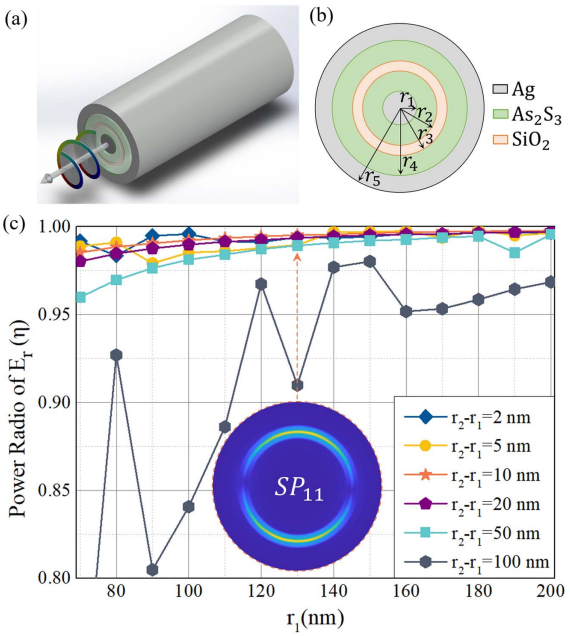

Fig. 1. (a) Schematic diagram of the plasmonic OAM waveguide; (b) cross-section of the OAM waveguide; (c) energy percentage of the radial polarization component E_r of the surface plasmon mode SP_{11}. Inset is the intensity distribution of the SP_{11} mode.

layers and two metal claddings. Because most energy is located in the middle low-index dielectric layer, the mode propagation loss has a significant decrease, which enables a longer propagation range. Without loss of generality, we performed a proof-of-concept study in which SiO_2, As_2S_3, and Ag are chosen as the constructional materials of the dielectric ring-core, dielectric claddings, and metal claddings, respectively.

In order to investigate the deep regulation of OAM mode below the diffraction limit, the guiding properties have been studied by using the finite element method at the telecommunication wavelength of 1550 nm. The model equation is $\nabla \times (\nabla \times E) - k_0^2 \varepsilon_r E = 0$, where E is the electric field, k_0 is the wave vector in vacuum, and ε_r represents the permittivity distributions of simulation model. The perfectly matched boundary conditions are used. The inset of Fig. 1(c) shows the electrical field distributions of the surface plasmon mode SP_{11} in the proposed OAM nano-waveguide with $r_1 = 130$ nm, $r_2 - r_1 = 10$ nm, $r_3 - r_2 = 5$ nm, $r_4 - r_3 = 10$ nm, and $r_5 - r_4 = 50$ nm. This result is consistent with the design expectation, that is, most of the mode energy is located into the SiO_2 channel. Less energy is distributed in two adjacent As_2S_3 layers, and no energy is diffused into the Ag layers. The SP_{11} mode is radially polarized because the electric field component parallel to the metal–dielectric interface incurs great transmission loss. As shown in Fig. 1(c), when $r_2 - r_1 \leq 50$ nm, the energy percentage of the radial polarization component E_r of the SP_{11} mode is always higher than 95% in the nano-waveguides with different r_1. Higher-order SP modes also have similar radial polarization state in this cylindrical hybrid plasmonic waveguide.

For synthesizing the OAM modes in the proposed nanowaveguide, the expression of E_r of the *SP* modes is analytically derived. The longitudinal electromagnetic fields (E_z and H_z) satisfy the following equations in a cylindrical coordinate system[30]:

$$\frac{\partial^2\Psi}{\partial r^2}+\frac{1}{r}\frac{\partial\Psi}{\partial r}+\frac{1}{r^2}\frac{\partial^2\Psi}{\partial\varphi^2}+\{k^2[n(r)]^2-\beta^2\}\Psi=0, \tag{1}$$

where Ψ, k, $n(r)$, and β are the longitudinal electromagnetic fields (E_z or H_z) of the SP modes, wave-number, refractive index profile, and propagation constant, respectively. Based on the variable separation method, E_z and H_z are expressed by

$$E_z=AF_{lm}(r)f(l\varphi), \tag{2}$$

$$H_z=CF_{lm}(r)g(l\varphi), \tag{3}$$

where A and C are the undetermined coefficients. $F_{lm}(r)$ is the radial dependence of the field profile. l and m are the azimuthal and radial mode orders. Due to the cylindrical symmetry, $f(l\varphi)$ can be the even and odd functions of the azimuth φ, which represent the even and odd modes, respectively. Accordingly, $g(l\varphi)$ will be the odd and even functions of the azimuth φ,

$$f(l\varphi)=\begin{cases}\cos(l\varphi) & \text{even modes}\\ \sin(l\varphi) & \text{odd modes}\end{cases}, \tag{4}$$

$$g(l\varphi)=\begin{cases}-\sin(l\varphi) & \text{even modes}\\ \cos(l\varphi) & \text{odd modes}\end{cases}. \tag{5}$$

The transverse electromagnetic field (E_r) can be obtained by E_z and H_z[16],

$$E_r=-\frac{j}{k^2[n(r)]^2-\beta^2}\left(\beta\frac{\partial E_z}{\partial r}+\frac{\omega\mu_0}{r}\frac{\partial H_z}{\partial\varphi}\right). \tag{6}$$

By substituting Eqs. (2) and (3) into Eq. (6), the E_r expressions of the even and odd SP_{lm} modes are

$$E_r^e=-\frac{j}{k^2[n(r)]^2-\beta^2}G_{lm}(r)\cdot\cos(l\varphi), \tag{7}$$

$$E_r^o=-\frac{j}{k^2[n(r)]^2-\beta^2}G_{lm}(r)\cdot\sin(l\varphi), \tag{8}$$

where

$$G_{lm}(r)=\beta A\frac{\partial F_{lm}(r)}{\partial r}-\frac{\omega\mu_0}{r}ClF_{lm}(r). \tag{9}$$

By superimposing Eqs. (7) and (8), the helical phase $\exp(\pm jl\varphi)$ is obtained,

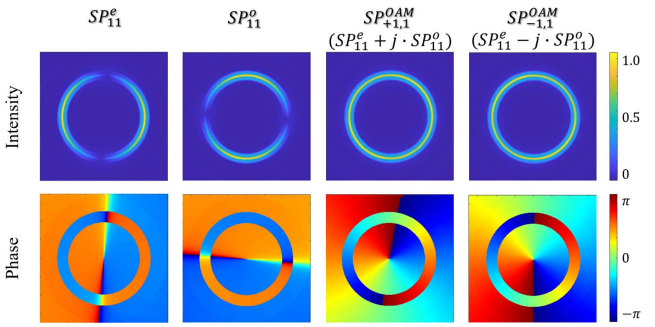

Fig. 2. Intensity and phase distributions of SP_{11}^{e}, SP_{11}^{o}, $\mathrm{SP}_{+1,1}^{\mathrm{OAM}}$, and $\mathrm{SP}_{-1,1}^{\mathrm{OAM}}$ modes.

$$E_r^e\pm j\cdot E_r^o=-\frac{j}{k^2[n(r)]^2-\beta^2}G_{lm}(r)\cdot\exp(\pm jl\varphi). \tag{10}$$

Therefore, the OAM plasmonic mode synthetic formula is

$$\mathrm{SP}_{\pm l,m}^{\mathrm{OAM}}=\mathrm{SP}_{lm}^{e}\pm j\cdot\mathrm{SP}_{lm}^{o}. \tag{11}$$

It is worth emphasizing that the synthetic formulas of the radially polarized OAM SP modes are different from the OAM modes in ring fiber. In the cylindrical hybrid plasmonic waveguide, the SP_{11} mode can achieve the first-order OAM mode, and high-order SP modes (SP_{lm}) can achieve OAM modes with the topological charge $\pm l$. Figure 2 shows the intensity and phase distributions of $\mathrm{SP}_{\pm1,1}^{\mathrm{OAM}}$ mode, which are obtained by $\mathrm{SP}_{11}^{e}\pm j\cdot\mathrm{SP}_{11}^{o}$. The uniform distributions of the doughnut-shaped intensity profile and the angular gradient phase indicate that the purity of the synthesized $\mathrm{SP}_{+1,1}^{\mathrm{OAM}}$ mode is nearly 100%. The $\mathrm{SP}_{-1,1}^{\mathrm{OAM}}$ mode has similar results, as shown in Fig. 2. The modal effective index difference between the SP_{11}^{e} and SP_{11}^{o} modes is $\Delta n_{\mathrm{eff}}=1\times10^{-7}$, where the related 2π walk-off length is $L_{2\pi}=\lambda/\Delta n_{\mathrm{eff}}=15.5$ m. The $\mathrm{SP}_{\pm1,1}^{\mathrm{OAM}}$ mode keeps stable during its propagation length of tens of micrometers.

3. Results

To further understand the $\mathrm{SP}_{+1,1}^{\mathrm{OAM}}$ mode in the proposed nanowaveguide, the effect of the waveguide size on the modal properties of $\mathrm{SP}_{+1,1}^{\mathrm{OAM}}$ mode is investigated. In Fig. 3(a), the modal effective index n_{eff} of $\mathrm{SP}_{+1,1}^{\mathrm{OAM}}$ mode increases with the increase of the radii of inner Ag cladding (r_1), which is consistent with the modal effective index of the fundamental mode in all-dielectric waveguides. When increasing the thickness of the As_2S_3 layer, the modal effective index decreases, which means the mode is less affected by the Ag cladding and becomes more concentrated in the dielectric layer.

The spatial constraint ability of $\mathrm{SP}_{+1,1}^{\mathrm{OAM}}$ mode is evaluated by the normalized mode area A_{norm}, which is defined as the ratio of the effective mode area A_{eff} to the diffraction-limited area A_0,

$$A_{\mathrm{norm}}=A_{\mathrm{eff}}/A_0, \tag{12}$$

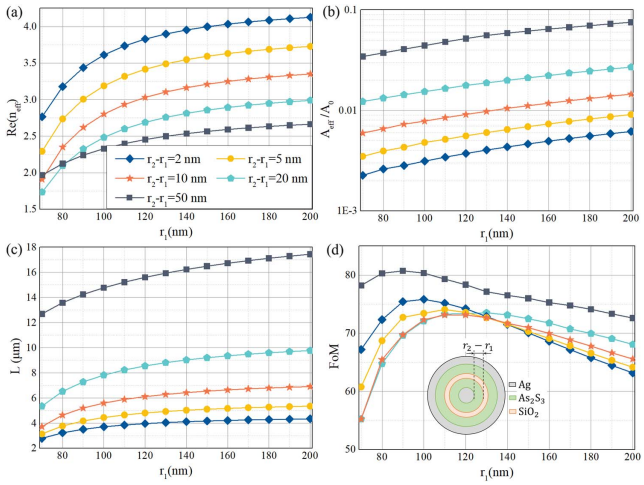

Fig. 3. Mode properties of $SP_{+1,1}^{OAM}$ mode in the nano-waveguides with $r_3 - r_2$ = 5 nm, $r_4 - r_3 = r_2 - r_1$, and $r_5 - r_4$ = 50 nm. (a) Modal effective index; (b) normalized mode area; (c) propagation length; (d) FoM. The inset is the cross-section of the OAM waveguide, where the thickness of the As_2S_3 layer is denoted as $r_2 - r_1$.

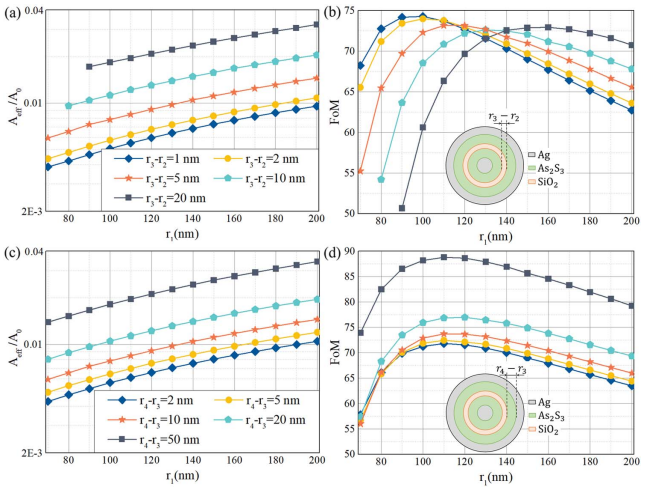

Fig. 4. (a) Normalized mode area and (b) FoM of $SP_{+1,1}^{OAM}$ modes in the nano-waveguides with $r_4 - r_3 = r_2 - r_1$ = 10 nm and $r_5 - r_4$ = 50 nm. Inset in (b) denotes the thickness of SiO_2 layer as $r_3 - r_2$. (c) Normalized mode area and (d) FoM of $SP_{+1,1}^{OAM}$ modes in the nano-waveguides with $r_2 - r_1$ = 10 nm, $r_3 - r_2$ = 5 nm, and $r_5 - r_4$ = 50 nm. Inset in (d) denotes the thickness of the outer As_2S_3 layer as $r_4 - r_3$.

$$A_{\text{eff}} = \iint P(r)\mathrm{d}A/\mathrm{Max}[P(r)], \tag{13}$$

$$A_0 = \lambda^2/4, \tag{14}$$

where $P(r)$ is the energy flux density and λ is the telecommunication wavelength of 1550 nm. As shown in Fig. 3(b), the $SP_{+1,1}^{OAM}$ mode can be confined at a very small area of $0.002A_0 = 0.0005\lambda^2$, outperforming many other OAM waveguides. Due to the tiny mode area, the modal properties of the proposed OAM nano-waveguide will be sensitive to environmental variations. On one hand, the stability of the OAM waveguide and the associated photonic devices will be affected, but on the other hand, the waveguide has potential for achieving ultra-high sensitivity sensors. Actually, such strongly constrained $SP_{+1,1}^{OAM}$ modes still suffer from optical loss because a small amount of energy locates at the Ag interface. The mode propagation loss is about 0.62–1.15 dB/μm, which is less than half that in existing OAM plasmonic waveguides[23]. The propagation length of the proposed nano-waveguide is defined as

$$L = \lambda/[4\pi \cdot \mathrm{Im}(n_{\text{eff}})]. \tag{15}$$

As shown in Fig. 3(c), the propagation length L can increase from 3 μm to 17.5 μm (2λ to 11λ) when the thickness of the As_2S_3 layer increases from 2 nm to 50 nm.

Since the mode localization and attenuation show the opposite trend, the FoM is used as an intuitive parameter for evaluating the guiding performances of waveguides. The FoM is defined as the ratio of propagation length to the diameter of the mode area,

$$\mathrm{FoM} = \frac{L}{2} \cdot \sqrt{\frac{\pi}{A_{\text{eff}}}}. \tag{16}$$

In Fig. 3(d), FoM has a non-monotonic behavior and reaches its maximum 81 with $r_1 = 90$ nm, $r_3 - r_2 = 5$ nm, and $r_2 - r_1 = r_4 - r_3 = r_5 - r_4 = 50$ nm.

Next, the effects of the thickness of the SiO_2 layer ($r_3 - r_2$) and outer As_2S_3 layer ($r_4 - r_3$) on the $SP_{+1,1}^{OAM}$ mode's performances are explored. Because most mode energy is concentrated in the SiO_2 layer, when decreasing the SiO_2 layer thickness, the normalized mode area and the propagation length of the $SP_{+1,1}^{OAM}$ mode both decrease [Fig. 4(a)]. The FoMs of the nano-waveguides can exceed 70 [Fig. 4(b)] with different thicknesses of the SiO_2 layer. When increasing the outer As_2S_3 layer thickness, the mode energy located in the outer As_2S_3 layer increases, which increases the normalized mode area of $SP_{+1,1}^{OAM}$ mode [Fig. 4(c)]. At the same time, the $SP_{+1,1}^{OAM}$ mode will be less affected by the outer Ag cladding, which greatly decreases mode loss and achieves an FoM of 88 [Fig. 4(d)].

The FoMs of the proposed nano-waveguide are further compared with three kinds of OAM cylindrical plasmonic waveguides: the Ag nanowire (Model 1), the Ag nanotube (Model 2), and hybrid plasmonic waveguides with the dielectric ring-core channel (Model 3). As shown in Fig. 5, under conditions of the same radii of inner Ag layer, the $SP_{+1,1}^{OAM}$ mode in our proposed waveguide has the largest FoM, which is about 4 times the FoM in Model 1 and 2 times the FoM in Model 3. In Model 2, the plasmonic OAM mode can only be propagated in the waveguide with the As_2S_3 core radii $r_1 \geq 180$ nm, which has disadvantage in waveguide miniaturization. These results illustrate that our proposed OAM nano-waveguide is highly promising

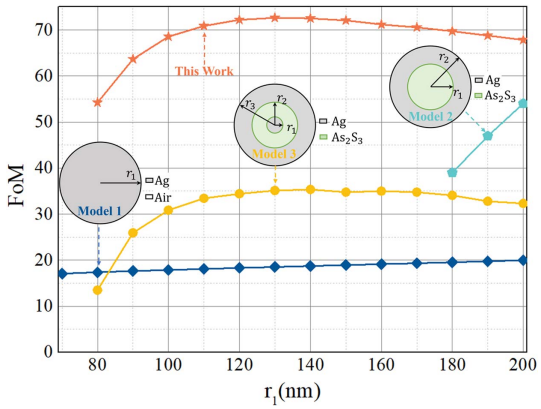

Fig. 5. FoM of the $SP_{+1,1}^{OAM}$ mode in four kinds of the nano-waveguides: the Ag nanowire (Model 1), the Ag nanotube (Model 2), the ring-core hybrid waveguide (Model 3), and this work.

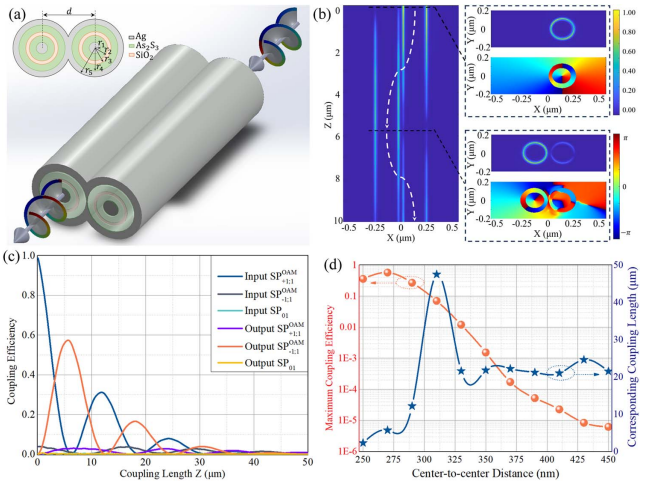

Fig. 6. (a) Schematic diagram of the plasmonic OAM waveguide coupler. (b) Propagating electric field of the $SP_{+1,1}^{OAM}$ mode coupler, where the white arrows represent the direction of optical energy flow. The upper dashed block diagram is the electric field and phase distribution of input $SP_{+1,1}^{OAM}$ mode. The lower dashed block diagram is the electric field and phase distribution of coupling mode with the maximum coupling efficiency. (c) Coupling efficiencies of different modes in the $SP_{+1,1}^{OAM}$ mode coupler. (d) Maximum coupling efficiency and corresponding coupling length of the $SP_{+1,1}^{OAM}$ mode coupler with different center-to-center distances.

for achieving the subwavelength OAM mode guiding and exhibits great potential in future on-chip OAM devices.

The OAM waveguide coupler within a small footprint is highly desired for chip-scale OAM applications. Based on the proposed subwavelength waveguide, the compact OAM coupler is composed of two parallel identical hybrid plasmonic waveguides, where the Ag claddings are fused together with a gap between two annular As_2S_3 layers. Without losing generality, the coupling characteristics of $SP_{+1,1}^{OAM}$ mode are investigated in the plasmonic coupler with $r_1 = 100$ nm, $r_2 - r_1 = 10$ nm, $r_3 - r_2 = 5$ nm, $r_4 - r_3 = 10$ nm, and $r_5 - r_4 = 50$ nm. The mode match method[31,32] is used for calculating the lossy high-order mode propagation through the coupling region. The key is that the two parallel waveguides are treated as a new uniform waveguide [Fig. 6(a)] and the coupling process is considered as the interference of the guide modes, which is decided by the overlapping coefficient of this mode and the input electrical field at the starting point of the coupling region, i.e., the injecting mode in the single input waveguide [Fig. 1(a)]. The coupling efficiencies of modes in the output waveguide are calculated at the end of the coupling region, which is similarly decided by the overlapping coefficients of the interference results and each mode in the single output waveguide.

Figure 6(b) shows the propagating electric field of the OAM plasmonic coupler with the center-to-center distance $d = 270$ nm. When injecting the annular $SP_{+1,1}^{OAM}$ mode, the cross-sectional electric fields are two parallel trajectories with reciprocating optical energy flow. The optimal coupling length is only 5.7 μm ($L = 3.68\lambda$). As shown in the lower dashed block diagram of Fig. 6(b), the coupled mode in the adjacent waveguide has a counterclockwise spiral phase, which means that the input $SP_{+1,1}^{OAM}$ mode has been coupled into the $SP_{-1,1}^{OAM}$ mode. The reason is that both $SP_{+1,1}^{OAM}$ and $SP_{-1,1}^{OAM}$ modes are the superposition of the SP_{11}^{e} and SP_{11}^{o} modes, but with a different phase difference. Due to the form birefringence of the coupling region, the SP_{11}^{e} and SP_{11}^{o} modes have different propagation constants, which induces an additional phase difference of π for turning the $SP_{+1,1}^{OAM}$ mode into the $SP_{-1,1}^{OAM}$ mode. As shown in Fig. 6(c), the peaks of the coupling efficiency curves decrease exponentially with the increase of coupling length z because of the transmission loss characteristics of the hybrid plasmonic waveguides. When the coupling length is 5.7 μm, the adjacent waveguide has a maximum coupling efficiency 57.37%. It is worth noting that, although the fundamental mode (SP_{01} mode) is excited due to the strong coupling effect, the mode purity of $SP_{-1,1}^{OAM}$ mode in the adjacent waveguide is still up to 95.22% by controlling the center-to-center distance. The presented design of the OAM plasmonic coupler has achieved an extremely small footprint of 0.68 μm × 5.7 μm, which shows an improvement of over 2 orders of magnitude compared to traditional OAM devices, such as the OAM microfiber coupler (10 μm × 25,000 μm)[31] and the OAM waveguide generator (4 μm × 100 μm)[33]. It is also noteworthy that the proposed coupler can be further expanded to the mode-selective coupler, which is widely used for efficiently generating the OAM mode from the fundamental mode, and converting the light to other OAM modes in waveguides.

The crosstalk between two adjacent OAM plasmonic waveguides is investigated in Fig. 6(d). When increasing the center-to-center distance d, the coupling effect is weakened, and the critical coupling length is increased. Considering that the plasmonic waveguides are highly lossy, the maximum coupling efficiency has decreased dramatically. For tightly arranged waveguides with $d = 350$ nm, the maximum coupling efficiency is only 0.15%, and the crosstalk is −28.14 dB. This result confirms that the proposed OAM nano-waveguide can be further applied to achieve high-density photonic circuits.

4. Discussion

The proposed nano-waveguide can be fabricated as follows. The silver nanowires can be synthesized via a two-step polyol process[34]. The As_2S_3 and SiO_2 layers can be prepared via the Stober method[34]. By changing the concentration of the As and Si ion solution, the dielectric layer thickness can be controlled on a nanoscale. The outer Ag layer can be prepared by an ion sputtering process. Additionally, the key to the proposed nano-waveguide is the metal–dielectric–metal structure, which means that the composite materials can be easily replaced according to the realizable preparation conditions and practical applications.

Considering the possible fabrication imperfections, such as the offset and elliptical transformation of the SiO_2 channel in OAM waveguide, the performances of $SP^{OAM}_{\pm1,1}$ mode in 10 μm waveguides [parameters as shown in the inset of Fig. 1(c)] have been studied. The modes still have doughnut-shaped intensity profiles with high FoMs (68 to 80). However, an additional phase $\Delta\Phi$ between the SP^{e}_{11} and SP^{o}_{11} modes will be induced due to the form birefringence. By taking $\Delta\Phi \le 0.05\pi$ as the criterion, the tolerances of the SiO_2 channel are the offset $\Delta x \le 9$ nm and the elliptical axis difference $-2\,\text{nm} \le \Delta r \le 2$ nm.

The proposed waveguide can support higher-order OAM mode by simply increasing its size. For example, the OAM nano-waveguide ($r_1 = 150$ nm, $r_2 - r_1 = 10$ nm, $r_3 - r_2 = 5$ nm, $r_4 - r_3 = 10$ nm, and $r_5 - r_4 = 50$ nm) supports OAM modes with $l = \pm2$, as shown in Fig. 7. This $SP^{OAM}_{+2,1}$ mode has a mode area of $0.012\lambda^2$ and a propagation length of 2.43λ. The parameter sweep analysis method will further improve waveguide performances. It is also worth noting that the proposed waveguide also keeps the small mode area of $SP^{OAM}_{\pm1,1}$ modes and FoM ≥ 60 in a broader range of wavelengths (from 900 to 2300 nm). Due to the tiny mode area, the proposed OAM nano-waveguide has a larger nonlinearity, which has potential for constructing the nonlinear device and generating the OAM mode with a new frequency.

In conclusion, we have proposed a novel cylindrical hybrid plasmonic waveguide for propagating the OAM mode beyond the diffraction limits. The OAM nano-waveguide consists of a SiO_2 ring-core, two As_2S_3 claddings, and two Ag claddings. The plasmonic OAM modes are tightly restricted in the SiO_2 ring-core channel and simultaneously realize the radial polarization state, a small mode area ($0.0005\lambda^2$), and a long propagation range (2λ to 11λ). Compared with traditional OAM plasmonic waveguides, the $SP^{OAM}_{\pm1,1}$ mode in the proposed waveguide has a larger FoM of 88. Based on this waveguide, a directional coupler with an extremely small footprint (0.68 μm × 5.7 μm) is designed, which has a maximum coupling efficiency of 57.37%. Due to the strong mode confinement, the crosstalk between two tightly arranged waveguides is down to −28.14 dB. The waveguide also can realize a transmission of the higher-order OAM mode in a broadband wavelength range. These results illustrate that our proposed OAM nano-waveguide is highly promising for achieving the high-performance of OAM mode guiding and exhibits great potential in future on-chip OAM devices.

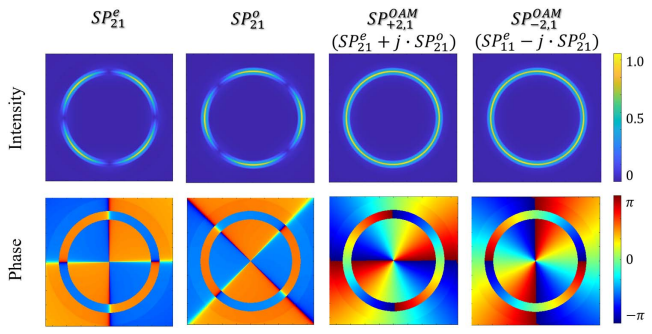

Fig. 7. Intensity and phase distributions of SP^{e}_{21}, SP^{o}_{21}, $SP^{OAM}_{+2,1}$, and $SP^{OAM}_{-2,1}$ modes in the waveguide with r_1 = 150 nm.

Acknowledgements

This work was supported by the National Natural Science Foundation of China (No. 62305057), the Guangdong Basic and Applied Basic Research Foundation (Nos. 2021B1515020095, 2021A1515110919, and 2019A1515110243), and the Research Fund of Guangdong-Hong Kong-Macao Joint Laboratory for Intelligent Micro-Nano Optoelectronic Technology (No. 2020B1212030010).

References

1. H. C. Zhang, L. P. Zhang, P. H. He, *et al.*, "A plasmonic route for the integrated wireless communication of subdiffraction-limited signals," Light Sci. Appl. **9**, 113 (2020).
2. X. Ou, Y. Yang, F. Sun, *et al.*, "Wide-range, ultra-compact, and high-sensitivity ring resonator biochemical sensor with CMOS-compatible hybrid plasmonic waveguide," Opt. Express **29**, 19058 (2021).
3. Y. Li and C. Argyropoulos, "Multiqubit entanglement and quantum phase gates with epsilon-near-zero plasmonic waveguides," Appl. Phys. Lett. **119**, 211104 (2021).
4. J. Zhang, Y. Kang, X. Guo, *et al.*, "High-power continuous-wave optical waveguiding in a silica micro/nanofibre," Light Sci. Appl. **12**, 89 (2023).
5. Y. Fang and M. Sun, "Nanoplasmonic waveguides: towards applications in integrated nanophotonic circuits," Light Sci. Appl. **4**, e294 (2015).
6. S. Kim and R. Yan, "Recent developments in photonic, plasmonic and hybrid nanowire waveguides," J. Mater. Chem. C **6**, 11795 (2018).
7. Á. Barreda, F. Vitale, A. E. Minovich, *et al.*, "Applications of hybrid metal-dielectric nanostructures: state of the art," Adv. Photonics Res. **3**, 2100286 (2022).
8. J. Yao, H. Fang, Y. Li, *et al.*, "Superplastic nanomolding of aluminum waveguides for subwavelength light routing, splitting, and encryption," ACS Nano **17**, 17342 (2023).
9. C. L. Smith, N. Stenger, A. Kristensen, *et al.*, "Gap and channeled plasmons in tapered grooves: a review," Nanoscale **7**, 9355 (2015).
10. Y. Bian, Q. Ren, L. Kang, *et al.*, "Deep-subwavelength light transmission in hybrid nanowire-loaded silicon nano-rib waveguides," Photon. Res. **6**, 37 (2018).
11. C.-C. Huang, R.-J. Chang, and C.-C. Huang, "Nanostructured hybrid plasmonic waveguide in a slot structure for high-performance light transmission," Opt. Express **29**, 29341 (2021).
12. M. Ono, M. Hata, M. Tsunekawa, *et al.*, "Ultrafast and energy-efficient all-optical switching with graphene-loaded deep-subwavelength plasmonic waveguides," Nat. Photonics **14**, 37 (2020).
13. J. Wang, J. Liu, S. Li, *et al.*, "Orbital angular momentum and beyond in free-space optical communications," Nanophotonics **11**, 645 (2022).

14. S. Liu, Y. Lou, and J. Jing, "Orbital angular momentum multiplexed deterministic all-optical quantum teleportation," Nat. Commun. **11**, 3875 (2020).
15. B. B. Yousif and E. E. Elsayed, "Performance enhancement of an orbital-angular-momentum-multiplexed free-space optical link under atmospheric turbulence effects using spatial-mode multiplexing and hybrid diversity based on adaptive MIMO equalization," IEEE Access **7**, 84401 (2019).
16. E. E. Elsayed and B. B. Yousif, "Performance enhancement of the average spectral efficiency using an aperture averaging and spatial-coherence diversity based on the modified-PPM modulation for MISO FSO links," Opt. Commun. **463**, 125463 (2020).
17. E. E. Elsayed, "Atmospheric turbulence mitigation of MIMO-RF/FSO DWDM communication systems using advanced diversity multiplexing with hybrid N-SM/OMI M-ary spatial pulse-position modulation schemes," Opt. Commun. **562**, 130558 (2024).
18. Y. Weng and Z. Pan, "Orbital angular momentum based sensing and their applications: a review," J. Lightwave Technol. **41**, 2007 (2023).
19. D. Paul, D. K. Sharma, and G. V. P. Kumar, "Simultaneous detection of spin and orbital angular momentum of light through scattering from a single silver nanowire," Laser Photon. Rev. **16**, 2200049 (2022).
20. J. Wang, C. Cai, F. Cui, *et al.*, "Tailoring light on three-dimensional photonic chips: a platform for versatile OAM mode optical interconnects," Adv. Photonics **5**, 036004 (2023).
21. A. Liu, M. Wu, R. Zhuang, *et al.*, "On-chip generation of the reconfigurable orbital angular momentum with high order," Opt. Express **28**, 17957 (2020).
22. Z. Zhang, S. Gao, L. Zhang, *et al.*, "All-fiberized sorter for nondestructively splitting the orbital angular momentum modes," Opt. Commun. **560**, 130462 (2024).
23. F. C. Ni, Z. T. Xie, X.-D. Hu, *et al.*, "Selective angular momentum generator based on a graphene hybrid plasmonic waveguide," J. Lightwave Technol. **37**, 5486 (2019).
24. J. Lee and S. Kim, "Directional coupler design for orbital angular momentum mode-based photonic integrated circuits," Opt. Express **28**, 30085 (2020).
25. D. S. Han and M. S. Kang, "Reconfigurable generation of optical vortices based on forward stimulated intermodal Brillouin scattering in subwavelength-hole photonic waveguides," Photon. Res. **7**, 754 (2019).
26. Y. Wang, X. Ma, M. Pu, *et al.*, "Transfer of orbital angular momentum through sub-wavelength waveguides," Opt. Express **23**, 2857 (2015).
27. C. Huang, X. Chen, A. O. Oladipo, *et al.*, "Generation of subwavelength plasmonic nanovortices via helically corrugated metallic nanowires," Sci. Rep. **5**, 13089 (2015).
28. J.-W. Liaw, S.-Y. Mao, J.-Y. Luo, *et al.*, "Surface plasmon polaritons of higher-order mode and standing waves in metallic nanowires," Opt. Express **29**, 18876 (2021).
29. D. Garoli, P. Zilio, Y. Gorodetski, *et al.*, "Beaming of helical light from plasmonic vortices via adiabatically tapered nanotip," Nano Lett. **16**, 6636 (2016).
30. L. Tong, J. Lou, and E. Mazur, "Single-mode guiding properties of subwavelength-diameter silica and silicon wire waveguides," Opt. Express **12**, 1025 (2004).
31. Z. Zhang, J. Gan, X. Heng, *et al.*, "Low-crosstalk orbital angular momentum fiber coupler design," Opt. Express **25**, 11200 (2017).
32. Z. Zhang, J. Gan, X. Heng, *et al.*, "High order vector mode coupling mechanism based on mode matching method," J. Opt. **19**, 065702 (2017).
33. S. Zheng and J. Wang, "On-chip orbital angular momentum modes generator and (de)multiplexer based on trench silicon waveguides," Opt. Express **25**, 18492 (2017).
34. H. Gan, S. Li, Y. Zhang, *et al.*, "Electrospun composite polymer electrolyte membrane enabled with silica-coated silver nanowires," Eur. J. Inorg. Chem. **2021**, 4639 (2021).